BIOMECHANICS

A novel scoliosis instrumentation using special superelastic nickel–titanium shape memory rods: a biomechanical analysis using a calibrated computer model and data from a clinical trial

Xiaoyu Wang[1,2] · Kelvin Yeung[3] · Jason Pui Yin Cheung[3] · Johnson Yiu-Nam Lau[3] · Weichen Qi[3] · Kenneth Man-Chee Cheung[3] · Carl-Eric Aubin[1,2]

Abstract

Study design Biomechanical analysis of scoliosis instrumentation using superelastic Nickel–titanium shape memory (SNT) rods.

Objective To compare SNT with conventional Titanium (Ti) and Cobalt–chrome (Co–Cr) rods.

Summary of background data A clinical trial has documented comparable efficacy between two adolescent idiopathic scoliosis (AIS) cohorts instrumented using SNT versus conventional Ti rods. The shape memory and superelasticity of the SNT rod are thought to allow easy rod insertion, progressive curve correction, and correction from spinal tissue relaxation, but study is yet to be done to assess the effects of the shape memory and superelasticity.

Methods Instrumentations of AIS patients from the clinical trial were computationally simulated using SNT, Ti and Co–Cr rods (5.5 or 6 mm; 30°, 50° or 60° sagittal contouring angles; 0°, 25° or 50° coronal over-contouring angles). Curve correction, its improvement from stress relaxation in the spine, and loads in the instrumentation constructs were computed and compared.

Results The simulated main thoracic Cobb angles (MT) and thoracic kyphosis with the SNT rods were 4°–7° higher and 1°–2° lower than the Ti and Co–Cr rods, respectively. Bone–implant forces with Ti and Co–Cr rods were higher than the SNT rods by 84% and 130% at 18 °C and 35% and 65% at 37 °C, respectively ($p < 0.001$). Further corrections of the MT from the simulated stress relaxation in the spine were 4°–8° with the SNT rods versus 2°–5° with the Ti and Co–Cr rods ($p < 0.001$).

Conclusion This study concurs with clinical observation that the SNT rods are easier to insert and can result in similar correction to the conventional rods. The SNT rods allow significantly lower bone–implant forces and have the ability to take advantage of post-instrumentation correction as the tissues relax.

Keywords Biomechanical analysis · Adolescent idiopathic scoliosis · AIS · Instrumentation · Superelastic nickel–titanium · Shape memory · Spinal rod

✉ Kenneth Man-Chee Cheung
cheungmc@hku.hk

✉ Carl-Eric Aubin
carl-eric.aubin@polymtl.ca

Xiaoyu Wang
xiaoyu.wang@polymtl.ca

Kelvin Yeung
wkkyeung@hku.hk

Jason Pui Yin Cheung
jcheung98@hotmail.com

Johnson Yiu-Nam Lau
JohnsonYNLau@aol.com

Weichen Qi
weichen_qi@foxmail.com

[1] Department of Mechanical Engineering, Polytechnique Montreal, Downtown Station, P.O. Box 6079, Montreal, QC H3C 3A7, Canada

[2] Sainte-Justine University Hospital Center, 3175, Cote Sainte-Catherine Road, Montreal, QC H3T 1C5, Canada

[3] Department of Orthopaedics and Traumatology, The University of Hong Kong, Hong Kong SAR, China

Introduction

Spinal rod is a key component in instrumentation for severe adolescent Idiopathic Scoliosis (AIS) [1]; rods of higher strength and stiffness are increasingly used to improve deformity correction [2, 3]. Since the amount of correction is bounded by the inherent properties of the spine [4], rods of higher strength may still plastically deform in stiff curves with a higher risk of compromising the rod fatigue and the bone–implant interface strength [3, 5, 6]. Rods of high stiffness also have a very low range of elastic flexion. This makes them subject to unrecoverable plastic deformation under the combined deformity correction loads and the postoperative physiological loads, which may result in postoperative loss of correction. The small elastic flexion angle means that the shape of the rods remains unchanged with external loads reduced or even removed, allowing little correction from spinal tissue relaxation.

A superelastic nickel–titanium shape memory (SNT) rod has been developed and clinically tested in AIS instrumentation. The SNT rod has a distinctive phase-changing behavior with its austenite changed to martensite upon cooling below 20 °C and the inverse upon heating to a threshold temperature of 37 °C. It is highly malleable below 20 °C. Being kept in ice water before insertion, it can be shaped with ease by surgeons to match the spinal curve and be attached at all anchor points with far smaller forces than the conventional rods [7, 8]. When warmed to 37 °C, internal forces are generated in the SNT rod to recover its predesigned shape realized through thermal treatment (shape memory effect), resulting in gradual deformity correction. At 37 °C, the SNT rod is superelastic with a wide stress–strain curve plateau. Regardless of the deformation it undergoes, the corrective forces remain relatively constant. This makes it predictable and ideal for use in scoliosis instrumentation and correction from tissue relaxation. In addition to the customized heat treatment to optimize the phase-changing and mechanical properties for AIS instrumentation, a special surface-treatment process has been developed to address potential concerns with allergic reactions or even toxicities of nickel in humans [9]. The surface treatment process is called plasma immersion ion implantation, whereby a layer of titanium nitride is formed on the surface of the SNT rods to make them mechanically more durable and prevent nickel release [10–12]. The safety of the SNT rods with this surface treatment has been established in in vitro and animal studies with rabbit and goat models [13, 14].

A clinical trial using such SNT rod in AIS has been completed with AIS patients randomized to receive either SNT or titanium (Ti) rod; surgical outcomes with SNT rods were comparable to those with the conventional rods in terms of deformity correction [8]. However, little biomechanical data is available for surgeons to utilize the shape memory and superelasticity for optimal effects on deformity correction. The objective of this study was to assess the effects of the shape memory, superelasticity, and the spinal tissue relaxation on deformity correction and bone–implant loads in AIS instrumentation using the SNT rod.

Methods

This study was to complement a clinical trial using SNT rods in AIS instrumentation [8]. AIS patients enrolled in the trial were randomized into two groups to receive either instrumentation with SNT or Ti rods. Twelve patients were randomly selected, six from each of the two groups, to conduct this biomechanical investigation on SNT vs. Ti and Cobalt–Chrome (Co–Cr) rods. Preoperative and postoperative data of the patients were used to build computerized patient-specific models of the spines using previously developed techniques [15–18]. The models were used to assess instrumentations with rods of different diameters, contouring angles, and mechanical properties. Demographic data and geometric indices are presented in Table 1. Modeling details are presented in the following subsections.

Patient-specific biomechanical spine model

Geometric models of the patients were built using their preoperative radiographs and multi-view reconstruction techniques [19, 20]. Key anatomical landmarks on the bony structure of the spine were identified, *e.g.*, pedicles, vertebral endplate middle and corner points, and transverse and spinous process extremities. The 2D coordinates of these landmarks were computed which were then used to obtain their 3D coordinates in space using a self-calibration algorithm [19, 20]. The reconstruction process was completed by registering detailed vertebral and pelvic models using a free-form deformation technique [19, 20].

Different modeling and calibration techniques have been developed to study the biomechanics of the spine with each of them particularly adapted for specific research questions, e.g., finite element models, multibody models, or hybrid/combined models [17, 21, 22]. Because the focus of this study was to assess first-order AIS correction and the associated resultant forces on the instrumentation constructs, we used a validated deformable multi-body model of the instrumented spine [17] and made the assumption that the global deformation of the bony structures in AIS instrumentation could be negligible compared with those of the intervertebral disks and ligaments. Furthermore,

Table 1 Patient demographic data and geometric indices

Case No	Sex	Age	Weight (kg)	Height (cm)	Preoperative coronal Cobb angle		Thoracic kyphosis (°)
					Standing (°)	Fulcrum bending (°)	
1	F	18	39	146.3	42	7	11
2	M	19	58.5	177	47	23	50
3	M	16	54.5	182	67	39	21
4	F	18	45.5	161	53	28	− 2
5	M	19	47.5	167	51	20	12
6	M	16	41	164	58	21	23
7	M	12	46	164	68	23	12
8	F	12	52.5	166.5	54	33	14
9	F	17	59.5	166	55	17	26
10	F	15	43.2	148.5	53	24	29
11	F	17	44	164	49	16	25
12	F	14	45.5	160	63	30	23

we integrated flexible elements to represent the proper bone–screw interface and deformable behavior using experimentally derived properties [23]. Details of the spine model used in this study were described elsewhere [17], and are summarized here.

Using MD ADAMS 2011 (MSC Software, Santa Ana, CA), vertebrae from T1 through L5 and the pelvis were modeled as rigid bodies connected through multiple flexible elements corresponding to the intervertebral disc, anterior longitudinal ligament (ALL), posterior longitudinal ligament (PLL), ligamentum flavum (LF), intertransverse ligament (ITL), facet joint capsule (FC), and interspinous ligament (ISL) combined with supraspinous ligament (SSL). Six translational springs were modeled to, respectively, represent (1) ALL, (2) PLL, (3) LF, (4) left ITL, (5) right ITL, and (6) the combined effect of ISL and SSL. A general spring was used to represent the biomechanical effect of the intervertebral disc. The contributions of the rib cage were 40%, 35%, and 31%, respectively, in spinal flexion/extension, lateral bending, and axial rotation, which were incorporated to the stiffness matrix of the general spring [24]. The six translational springs were modeled as cable-like elements. Their stiffness in compression were set to null and those in traction were initially set using reported experiment results on cadaveric specimens, *e.g.,* 23.6 N/mm (ALL), 24.9 N/mm (PLL), 32.6 N/mm (LF), 12.9 N/mm (ITL), and 32.1 N/mm (ISL combined with SSL) [25–27]. The stiffness of the springs were then adapted to match the loading simulation results with the reported load–displacement data [28–30]. All model element stiffness were further adjusted such that fulcrum-bending simulations reproduced the Cobb angles measured on the patient's fulcrum-bending radiographs using a similar optimization technique reported in references [15, 31].

Instrumentation modeling and simulations

Since the deformations of the pedicle screws are negligible compared with intervertebral displacement in AIS correction, screw components were modeled as rigid body. The screw models were aligned with their corresponding vertebrae and bone–screw connections were modeled to simulate the flexible behavior using generalized 6-DOF stiffness elements whose mechanical properties were calibrated with load–displacement curves obtained through in-house experiments on instrumented cadaveric vertebrae [23]. Rods were modeled using deformable Timoshenko beam elements with user-defined mechanical property functions representing the rod materials tested in this study.

The SNT rods used in the clinical trial were prebent to 30° kyphosis in the thoracic portion with a customized heat treatment [13]. Mechanical tests were conducted to acquire stress–strain data of the SNT rods. The test set-up and typical load–displacement results are presented in Fig. 1. The patient-specific spine and instrumentation construct models were further calibrated by simulating the actual instrumentations with the simulation results within 5° of the actual surgical results in terms of Cobb angles in the coronal and sagittal planes. Preoperative radiographs and model views of the instrumentation simulation based on a sample case are provided in Fig. 2. For each patient, instrumentations with pedicle screws at alternate levels, SNT, Ti, and Co–Cr rods of different parameters were simulated. Surgical implant strategies vary with surgeons and practice, and there are published examples of use of this alternate level screw strategy [32–35]. Moreover, 75% of a group of experienced surgeons from the Minimize Implants Maximize Outcomes Study Group would use it as their preferred low screw
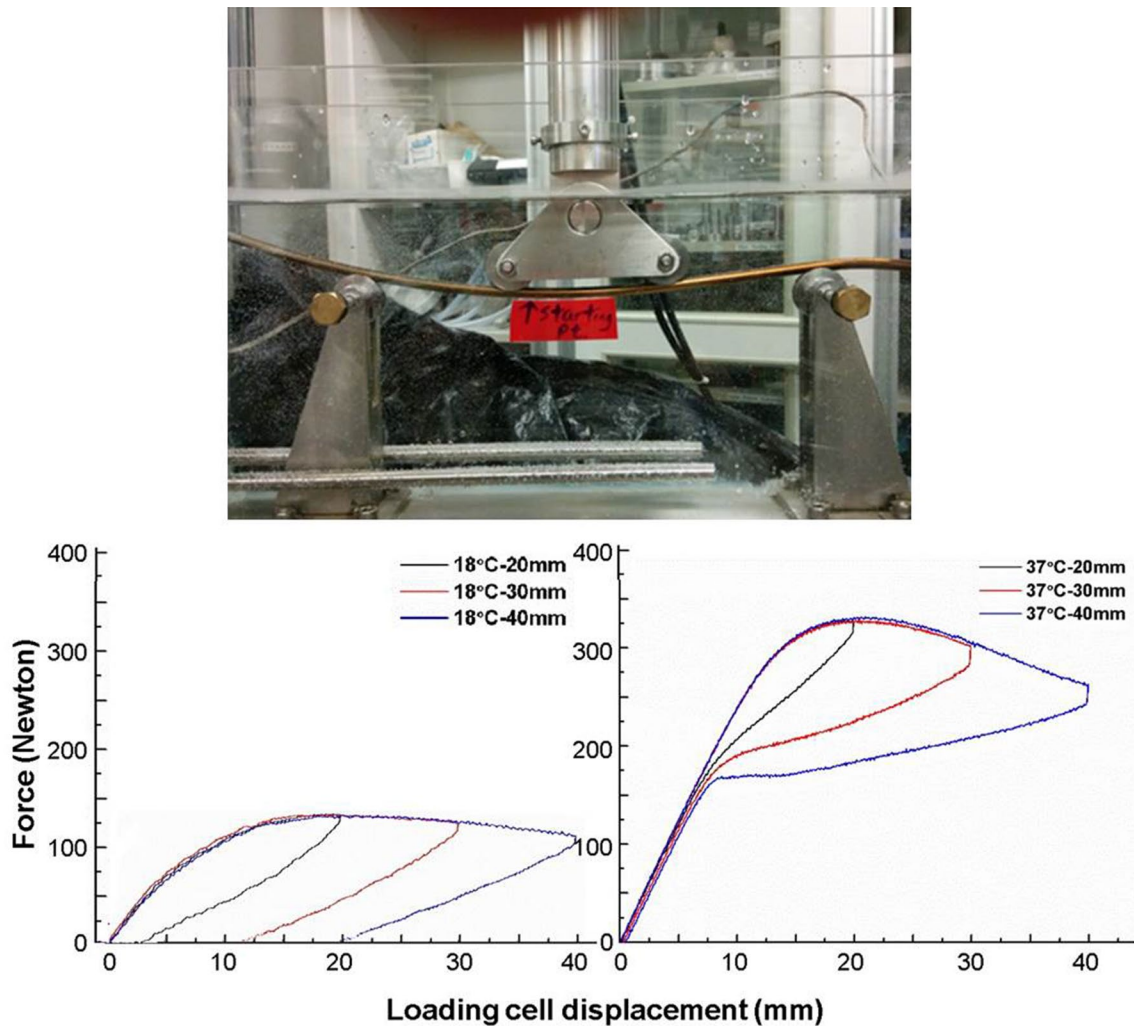
Fig. 1 Loading/unloading test set-up and typical results: Load–displacement curves in 4-point bending of 6-mm superelastic nickel–titanium shape memory rod as recorded by the Universal Testing Machine when loading to 20 mm, 30 mm, and 40 mm deflections of the loading cell, and then unloading to 0 Newton at 18 °C and 37 °C, respectively

density construct [32, 36, 37]. Other tested variables were rod diameter (5.5 and 6 mm), rod sagittal contouring angle (30°, 50° and 60°), and rod coronal over-contouring angle (contoured in the coronal plane opposite to the spinal curve) (0°, 25° and 50°). The SNT rod was simulated at 18 °C and 37 °C, respectively. The simulated correction maneuvers were segmental translation with rods locked at the distal ends of the instrumentation. Before the simulation of the final set-screw locking, 30% stress relaxation in the spine was simulated based on the biomechanical tests on human cadaveric spine assessing the extent of intervertebral stress relaxation [38]. For a total of 1512 simulations, the resulting main thoracic Cobb angle (MT), thoracic kyphosis (TK), and forces in the constructs were computed.

Results

Differences in the simulated MT and TK between the SNT, Ti, and Co–Cr rods can be appreciated with the comparison charts (Fig. 3). Before the simulated stress relaxation in the spine, differences between the SNT, Ti, and Co–Cr rods did not exceed 8° with the SNT rods having the least amount of correction of the major Cobb. SNT rods enabled about 5° more coronal corrections than the Ti and Co–Cr rods in the simulated stress relaxation of the spine. Overall, corrections with the three types of rods were clinically equivalent when taking into account corrections from spinal tissue relaxation (Fig. 4), i.e., differences did not exceed the accepted systematic error in clinical Cobb
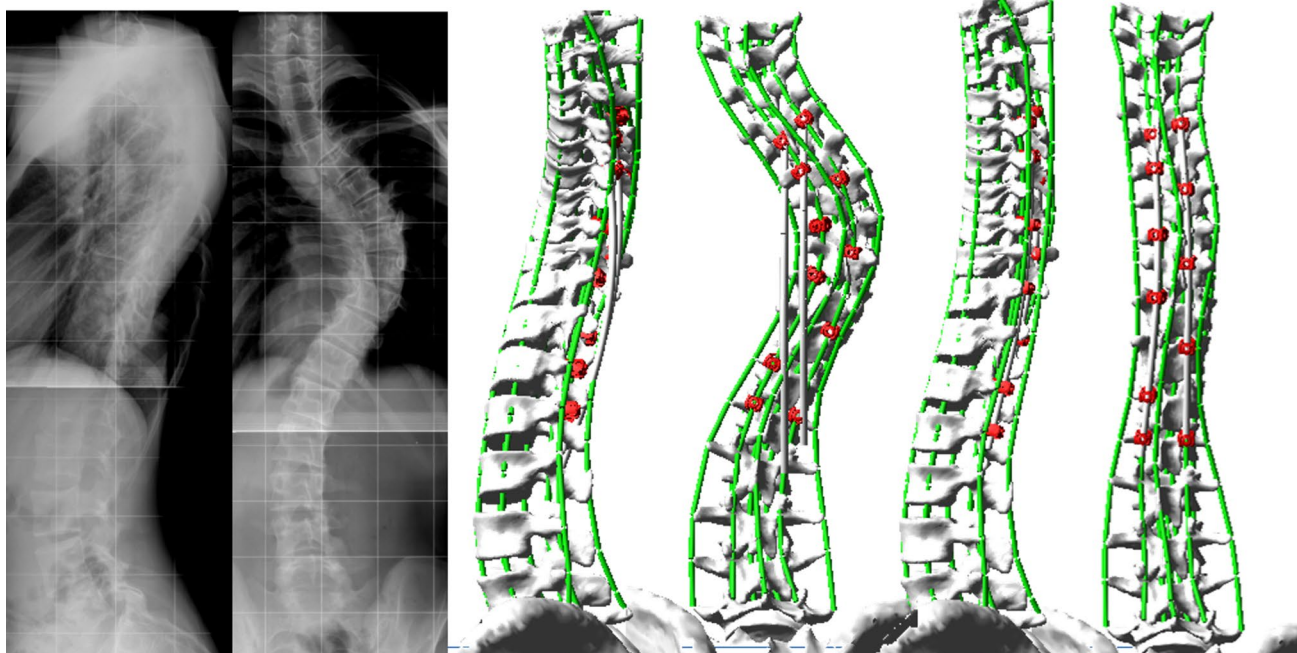
Fig. 2 Preoperative radiographs of Case No. 3 and model views of instrumentation simulation with 6.0-mm superelastic nickel–titanium shape memory rods and pedicle screws at alternate levels

Fig. 3 Simulated main thoracic Cobb angles and thoracic kyphosis (mean ± SD) with the superelastic nickel–titanium (SNT) shape memory, titanium, and cobalt–chrome 5.5- and 6.0-mm-diameter rods (before the simulated stress relaxation in the spine)
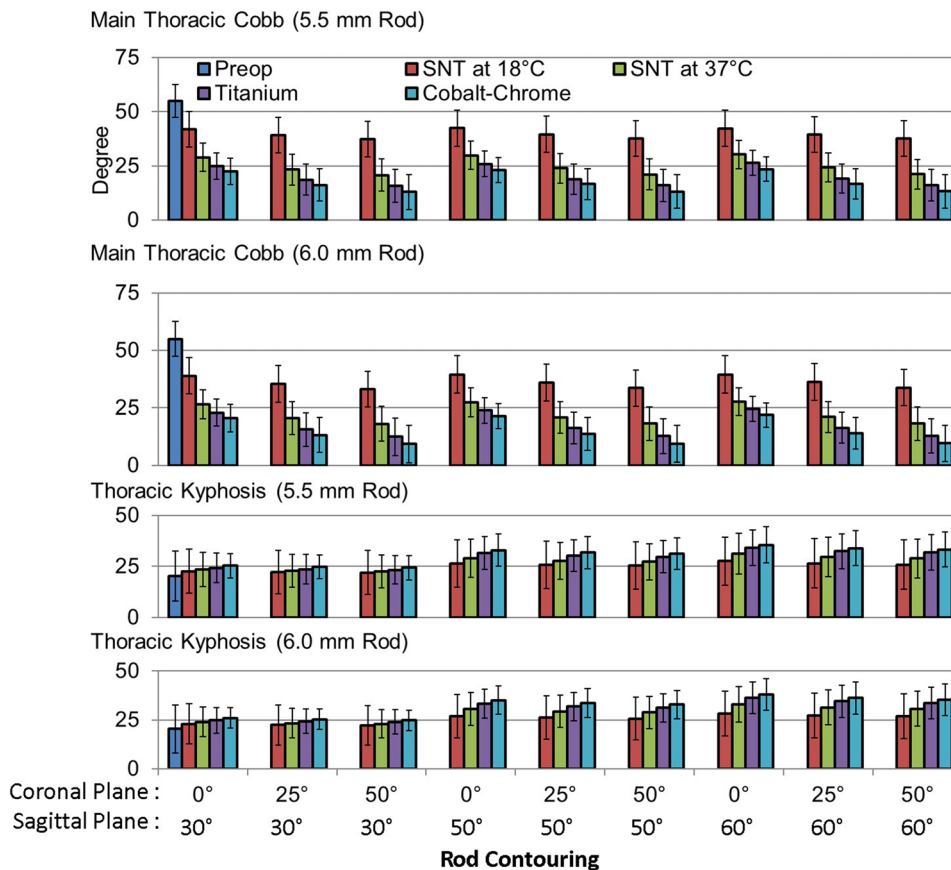
Fig. 4 Changes of the main thoracic Cobb angles and thoracic kyphosis (mean ± SD) after the simulated 30% stress relaxation in the spine model with the superelastic nickel–titanium (SNT) shape memory, titanium, and cobalt–chrome rods
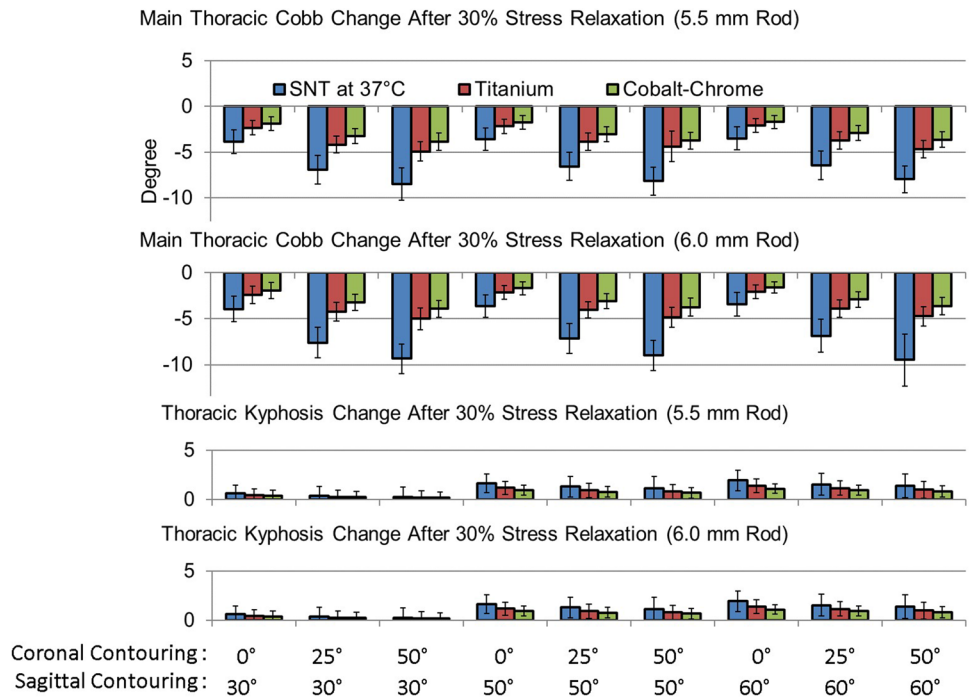

Fig. 5 Simulated bending moments (mean ± SD) in the superelastic nickel–titanium (SNT) shape memory, titanium, and cobalt–chrome rods
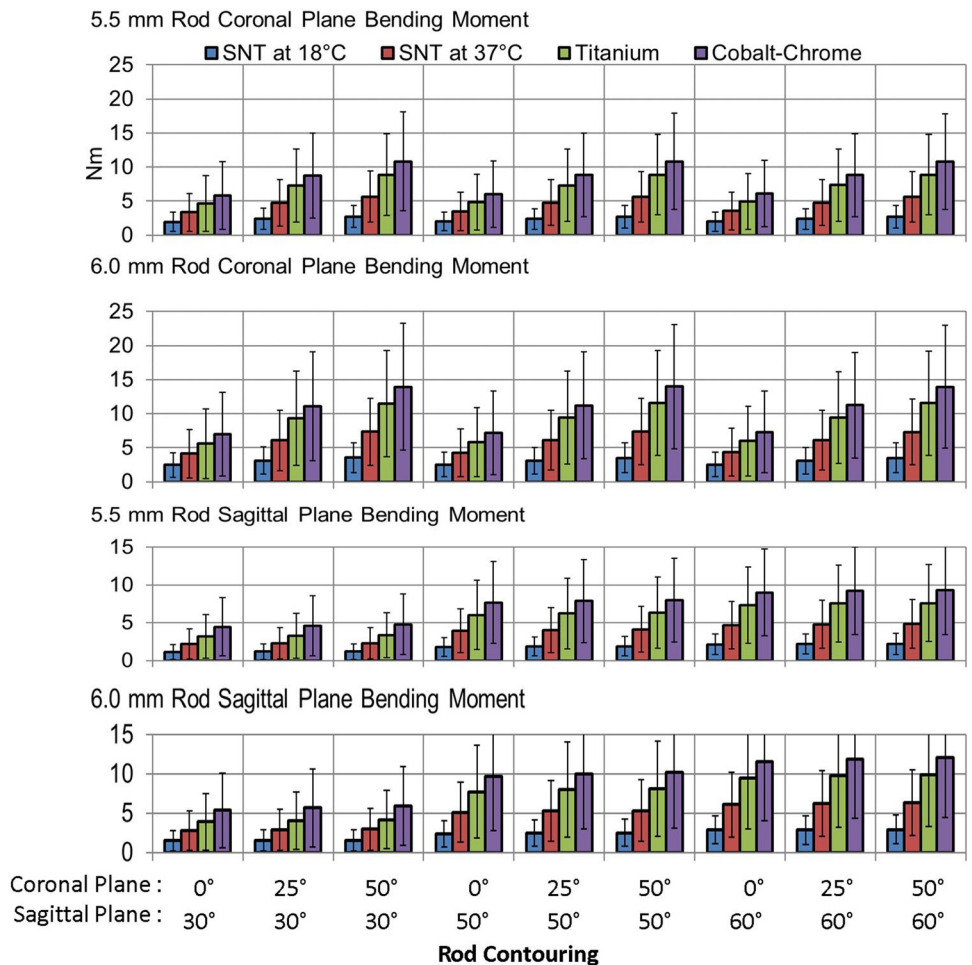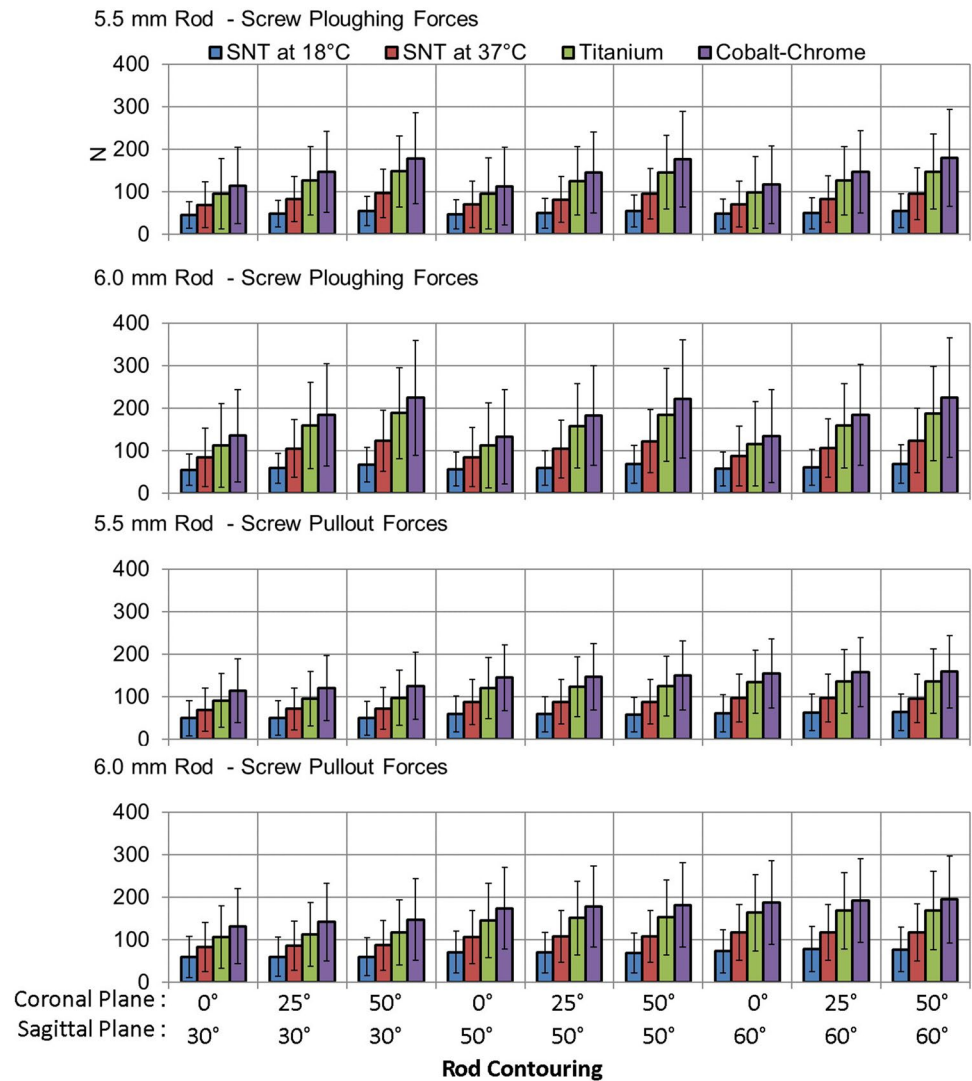
Fig. 6 Simulated bone–screw forces (mean ± SD) with the superelastic nickel–titanium (SNT) shape memory (SNT at 18 °C: forces during insertion; SNT at 37 °C: forces during reduction), titanium, and cobalt–chrome rods

angle measurements (5°) [39]. The comparison charts in Figs. 5 and 6 show that loads in the SNT constructs at the insertion temperature are less than half of the loads at the body temperature, suggesting that rod reduction can be completed with significantly smaller forces. They also show that loads in the SNT constructs were systematically lower than the Ti and Co–Cr constructs.

In 30°/0°/5.5 mm (rod sagittal/coronal contouring angles/diameter) instrumentations, the simulated MT with SNT rods were 42° ± 8° before the phase transformation and 29° ± 7° after the transformation, 4° and 7° higher than the Ti and Co–Cr rods, respectively (Fig. 3). The TK with the SNT rods were 23° ± 11° before the phase transformation and 24° ± 8 after the transformation, 1° and 2° lower than the Ti and Co–Cr rods, respectively. Coronal/sagittal plane bending moments in the SNT rods were 2 ± 1.4Nm/1.1 ± 1 Nm and 3.4 ± 2.8Nm/2.2 ± 2Nm before and after the phase transformation, respectively (Fig. 5). Screw plowing/pullout forces were, on average, 46 ± 31 N/50 ± 42 N and

70 ± 54 N/70 ± 50 N before and after the phase transformation, respectively (Fig. 6), which were all well below the clinically important threshold of pedicle screw fixation strength (700–800 N in pullout [40–42]). Bending moments in the Ti and Co–Cr rods were, respectively, 41% and 87% higher than the SNT rods at 37 °C ($p < 0.001$). Forces at the bone–screw interface with Ti and Co–Cr rods were, respectively, 84% and 130% higher than the SNT rods at 18°, and 35% and 65% higher than the SNT rods at 37 °C ($p < 0.001$). In the simulated stress relaxation, the MT with the SNT rods decreased by 4° ± 1° versus 2° ± 1° with Ti and Co–Cr rods ($p < 0.001$); the TK changes with all the three types of rods were less than 3° (Fig. 4).

In 30°/50°/5.5 mm instrumentations, the MT with SNT rods at 37 °C were 21° ± 7°, lower than the MT with Ti and Co–Cr rods in the 30°/0°/5.5 mm instrumentations (25° ± 6° and 22° ± 6°, respectively) ($p < 0.001$). With the same coronal plane over-contouring angle, the MT with SNT rods were about 4° and 7° higher than Ti and Co–Cr rods,

respectively. In 30°/50°/5.5 mm instrumentations, coronal plane bending moments in the SNT rods and screw plowing forces after the phase transformation were 5.6 ± 3.8 Nm and 97 ± 57 N. The coronal plane bending moments in the Ti and Co–Cr rods were, respectively, 57% and 92% higher than the SNT rods ($p < 0.001$); the screw plowing forces were, respectively, 53% and 85% higher than the SNT rods ($p < 0.001$). The peak forces with the Ti and Co–Cr rods were about 1200–1800 N when simulating rod attachment one screw at a time with a rod coronal over-contouring angle of 50°. In the simulated stress relaxation of the spine with a 50° rod coronal over-contouring angle, the MT with SNT rods decreased by $8° \pm 2°$ versus $5° \pm 1°$ and $4° \pm 1°$ with Ti and Co–Cr rods ($p < 0.001$).

In 60°/0°/5.5 mm instrumentations, the TK increased, on average, by 7°, 10°, and 11° with the SNT, Ti, and Co–Cr rods, respectively. Only at the 2–4 apical vertebral levels, were sagittal bending moments in the SNT rods higher than the threshold value for them to work in superelasticity. Increasing the rod diameter from 5.5 to 6 mm improved the coronal plane correction by around 4°, 5°, and 6° by the SNT, Ti, and Co–Cr rods, respectively; the effects on the TK were about 2°–5° for the three types of rods.

Discussions

Results from the current study provided insight into the biomechanics of AIS instrumentation using the SNT vs. Ti and Co–Cr rods, which agreed with the clinical trial results [8]. It shows that gradual curve correction is possible through the austenite phase transformation and tissue relaxation using the SNT rod, and that the results with the SNT rods are at least comparable to the Ti rods when using the same rod contouring angle and correction technique. The acquired biomechanical data bridged the knowledge gap to optimize instrumentation parameters to maximally utilize the unique material properties of the SNT rods.

Before the austenite phase transformation, the stiffness of the SNT rod was 36% of the Ti rod stiffness and 18% of the Co–Cr rod stiffness, while its yield strength was 27% of

the yield strength of the Ti and Co–Cr rod (Table 2). The lower stiffness and yield strength were reflected in the much lower forces at the bone–screw interface with the SNT rods before the austenite phase transformation (Fig. 6). This may clinically imply that the SNT rod reduction can be completed with much lower forces, which agreed with what was observed in the clinical trial [8]. After the austenite phase transformation, although the stiffness and plateau stress of the SNT rod are still lower than the Ti and Co–Cr rods, the MT with SNT rods were only 4° and 7° higher than the Ti and Co–Cr rods, respectively. This may be attributed to the non-linear sigmoid load–displacement properties of the spine. Within the range of motion (ROM) of the spine, especially within the neutral zone (a region of intervertebral motion with little resistance from the spine [43]), correction can be achieved with relatively lower forces [44], and the SNT rods could usually be as sufficient as the Ti and Co–Cr rods. When correction approaches the ROM, the stiffness of the spine become significantly higher; a small amount of correction will require much higher corrective forces. At the limits or beyond the ROM, the high stiffness and yield strength of Ti and Co–Cr rods could result in high bone–screw forces, but may not result in as much as correction. Clinical studies have also reported that correction improvement was not clinically significant using rods of higher stiffness [45, 46]. In contrast to the Ti and Co–Cr rods, the SNT rods allow relatively constant corrective forces with their wide loading stress–strain curve plateau regardless of the ROM of the spine, resulting in lower post-reduction bone–implant loads, which may provide additional benefits to reduce the risks of proximal junctional kyphosis due to postoperative implant pullout, bone and construct failure [47, 48].

In the coronal plane, corrective forces are obviously positively correlated with the rod over-contouring angle and the rod diameter. The simulation results showed that the SNT rods with an over-contouring of 50° allowed better MT corrections than the Ti and Co–Cr rods which had a coronal angle of 0°. One may argue that the SNT rods should be compared with the TI and Co–Cr rod having the same coronal angle. However, the simulated Ti and Co–Cr rods with

Table 2 Bending stiffness, threshold bending moment and angle (bending moment and angle at which plastic/superelastic deformation occur in Titanium and Cobalt–Chrome/Superelastic Nickel–Titanium (SNT) rods with a length of 100 mm)

	Diameter (mm)	SNT at 18 °C	SNT at 37 °C	Titanium	Cobalt–Chrome
Threshold Bending Moment (Nm)	5.5	3.51	7.99	12.94	12.95
	6	4.56	10.37	16.79	16.82
Threshold Bending Angle (°)	5.5	11.12	15.39	14.60	7.51
	6	10.19	14.11	13.39	6.88
Bending Stiffness (Nm/°)	5.5	0.32	0.52	0.89	1.72
	6	0.45	0.74	1.25	2.44

a coronal angle of 50° lead to 1200–1800 N bone–screw forces when connecting the rod to screws one at a time, which exceeded the bone–screw fixation strength [49, 50]. It should be pointed out that Ti or Co–Cr rod with a prebent coronal angle of 50° opposite to the spinal curve may result in bone–screw loads higher than the fixation strength and should be used with caution. Due to the low stiffness and yield strength before the austenite phase transformation, the SNT rods may be used with a relatively large coronal over-contouring angle without high bone–screw forces. Moreover, deformity correction using the SNT rod is mainly achieved through the austenite phase transformation during which the rods have already been captured at all screws such that corrective forces are spread over multiple anchor points. This is fundamentally different from correction using the Ti and Co–Cr rods achieved through rod attachment to one screw at a time with significantly higher transient load on the screw being attached to. Being superelastic, the predesigned contour of the SNT rods cannot be changed through in situ rod contouring. In future, it is envisaged that the rod design will be patient specific; the contour and correction force needed for maximum correction while reducing the risk of pullout of screws can be determined before surgery using computerized patient-specific model for spinal instrumentation simulation.

Correction from tissue relaxation depends on how much deformation the rod can recover when external loads are reduced or released, which is negatively correlated with the local slope of its load–displacement curve. Given the same amount of stress relaxation of the spine, the SNT rod can recover significantly more deformation than the Ti and Co–Cr rods due to its superelasticity. To utilize the superelasticity effectively, loads on the SNT rods should at least exceed the threshold value at which the superelastic deformation occurs. In the 30°/0°/6 mm instrumentations, bending moments in the SNT rods were mostly below the threshold value (Table 2 and Fig. 5) and the rods did not actually work in superelasticity, which may explain why the superelastic effects of the SNT rods were not clearly observed in the clinical trials. Over-contouring the SNT rods in the coronal plane to 50°, coronal rod bending moments exceeded the threshold value in all the cases over 4–6 vertebral levels, thus resulting in significantly higher correction improvement from simulated tissue relaxation.

The construct with pedicle screws at alternate levels tested in this study is only one of the commonly used low screw density constructs; there is wide variation in surgeon-preferred constructs [32, 51]. Different constructs may result in different corrections and bone–implant forces [32, 51, 52]. However, the mechanical contributions of one type of spinal rod vs another type of rod should be similar for different implant patterns. The present study was intended to better understand the biomechanics of spines instrumented using superelastic vs. standard elastoplastic rods, a reported low screw density construct was simulated, assuming that differences between instrumentations using the SNT vs Ti or Co–Cr rods with one construct should be similar to those with other constructs. In the future, such modeling tools could enable patient-specific optimal implant distribution, rod contours, and other instrumentation parameters for every patient.

Patient-specific model calibration was limited by the available preoperative spinal flexibility tests. The fulcrum-bending radiographs could only be used for the estimation of the ROM and the stiffness of the spine in the coronal plane. Since the focus was on the comparison between the SNT, Ti, and Co–Cr rods in terms of Cobb angles and resultant forces, which were overall evaluation indices, the models were, therefore, considered as adequate for this study. To establish baseline data for the customized stiffness, plateau stress, and contouring angles of the SNT rod, studies through simulations using computerized biomechanical models should be combined with more prospective clinical studies and mechanical experiments.

Conclusions

This study highlighted a few important points. First, the austenite phase-changing behavior of the SNT rod enabled rod attachment with significantly lower forces than the Ti and Co–Cr rods. Second, the shape memory of the SNT rods allowed gradual deformity correction after rods have already been attached to all screws spreading corrective forces over all anchor points. Corrections in the simulated AIS instrumentations using the SNT were comparable to the Ti and Co–Cr rods with significantly lower forces at the bone–screw interface. Third, the superelasticity of the SNT rods makes it possible to predict the maximal value of the corrective forces. The superelasticity of the SNT rods can be utilized for additional deformity correction as tissues relax. Also note that the stiffness at different phases and the loading and unloading plateau stresses of the SNT rods may be adapted to curves of different types and flexibilities through customized heat treatment to minimize the number of implants, which remains to be investigated in future studies.

Compliance with ethical standards

Conflict of interest All authors declare that they have no conflict of interest.

Ethical approval Approval of Research Ethics Committee was obtained to conduct this study.

References

1. Jada A, Mackel CE, Hwang SW et al (2017) Evaluation and management of adolescent idiopathic scoliosis: a review. Neurosurg Focus 43:E2
2. Prince DE, Matsumoto H, Chan CM et al (2014) The effect of rod diameter on correction of adolescent idiopathic scoliosis at two years follow-up. J Pediatr Orthop 34:22–28
3. Serhan H, Mhatre D, Newton P et al (2013) Would CoCr rods provide better correctional forces than stainless steel or titanium for rigid scoliosis curves? J Spine Disord Tech 26:E70–E74
4. Luk KD, Vidyadhara S, Lu DS et al (2010) Coupling between sagittal and frontal plane deformity correction in idiopathic thoracic scoliosis and its relationship with postoperative sagittal alignment. Spine 35:1158–1164
5. Cidambi KR, Glaser DA, Bastrom TP et al (2012) Postoperative changes in spinal rod contour in adolescent idiopathic scoliosis: an in vivo deformation study. Spine 37:1566–1572
6. Lindsey C, Deviren V, Xu Z et al (2006) The effects of rod contouring on spinal construct fatigue strength. Spine 31:1680–1687
7. Yeung KWK, Cheung KMC, Lu WW et al (2004) Optimization of thermal treatment parameters to alter austenitic phase transition temperature of NiTi alloy for medical implant. Mater Sci Eng A 383:213–218
8. Cheung JPY, Samartzis D, Yeung K et al (2018) A randomized double-blinded clinical trial to evaluate the safety and efficacy of a novel superelastic nickel-titanium spinal rod in adolescent idiopathic scoliosis: 5-year follow-up. Eur Spine J Off Publ Eur Spine Soc Eur Spinal Deform Soc Eur Sect Cerv Spine Res Soc 27:327–339
9. Kim YJ, Kassab F, Berven SH et al (2005) Serum levels of nickel and chromium after instrumented posterior spinal arthrodesis. Spine (Phila Pa 1976) 30:923–926
10. Liu XM, Wu SL, Chan YL et al (2007) Surface characteristics, biocompatibility, and mechanical properties of nickel-titanium plasma-implanted with nitrogen at different implantation voltages. J Biomed Mater Res A 82:469–478
11. Liu X, Wu S, Yeung KW et al (2011) Relationship between osseointegration and superelastic biomechanics in porous NiTi scaffolds. Biomaterials 32:330–338
12. Poon RW, Yeung KW, Liu XY et al (2005) Carbon plasma immersion ion implantation of nickel-titanium shape memory alloys. Biomaterials 26:2265–2272
13. Wu S, Liu X, Chan YL et al (2007) Nickel release behavior, cytocompatibility, and superelasticity of oxidized porous single-phase NiTi. J Biomed Mater Res A 81:948–955
14. Yeung KW, Poon RW, Chu PK et al (2007) Surface mechanical properties, corrosion resistance, and cytocompatibility of nitrogen plasma-implanted nickel-titanium alloys: a comparative study with commonly used medical grade materials. J Biomed Mater Res A 82:403–414
15. Aubin CE, Labelle H, Chevrefils C et al (2008) Preoperative planning simulator for spinal deformity surgeries. Spine 33:2143–2152
16. Wang X, Aubin CE, Coleman J et al (2017) Correction Capability in the 3 Anatomic Planes of Different Pedicle Screw Designs in Scoliosis Instrumentation. Clin Spine Surg 30:E323–E330
17. Wang X, Boyer L, Le Naveaux F et al (2016) How does differential rod contouring contribute to 3-dimensional correction and affect the bone-screw forces in adolescent idiopathic scoliosis instrumentation? Clin Biomech (Bristol, Avon) 39:115–121
18. Wang X, Larson AN, Crandall DG et al (2017) Biomechanical effect of pedicle screw distribution in AIS instrumentation using a segmental translation technique: computer modeling and simulation. Scoliosis Spinal Disord 12:13
19. Cheriet F, Laporte C, Kadoury S et al (2007) A novel system for thE 3-D reconstruction of the human spine and rib cage from biplanar X-ray images. IEEE Trans Biomed Eng 54:1356–1358
20. Cheriet F, Meunier J (1999) Self-calibration of a biplane X-ray imaging system for an optimal three dimensional reconstruction. Comput Med Imaging Graph 23:133–141
21. Wagnac E, Arnoux PJ, Garo A et al (2012) Finite element analysis of the influence of loading rate on a model of the full lumbar spine under dynamic loading conditions. Med Biol Eng Comput 50:903–915
22. Fradet L, Wang X, Crandall D et al (2018) Biomechanical analysis of acute proximal junctional failure after surgical instrumentation of adult spinal deformity: the impact of proximal implant type, osteotomy procedures, and lumbar lordosis restoration. Spine Deform 6:483–491
23. Wang X, Aubin CE, Crandall D et al (2012) Biomechanical analysis of 4 types of pedicle screws for scoliotic spine instrumentation. Spine (Phila Pa 1976) 37:E823–E835
24. Watkins RT, Watkins R, Williams L et al (2005) Stability provided by the sternum and rib cage in the thoracic spine. Spine 30:1283–1286
25. Myklebust JB, Pintar F, Yoganandan N et al (1988) Tensile strength of spinal ligaments. Spine (Phila Pa 1976) 13:526–531
26. Pintar FA (1986) The biomechanics of spinal elements (ligaments, vertebral body, disc). Ann Arbor: Marquette University, p 237.
27. Tong SYP (1999) A mechanical model of the normal human spine. Ann Arbor: University of Alberta (Canada), p 164
28. Gardner-Morse MG, Stokes IA (2004) Structural behavior of human lumbar spinal motion segments. J Biomech 37:205–212
29. Panjabi MM, Brand RA, Jr., White AA, 3rd. Mechanical properties of the human thoracic spine as shown by three-dimensional load-displacement curves. J Bone Joint Surg Am 58:642–52.
30. Panjabi MM, Oxland TR, Yamamoto I et al (1994) Mechanical behavior of the human lumbar and lumbosacral spine as shown by three-dimensional load-displacement curves. J Bone Joint Surg Am 76:413–424
31. Petit Y, Aubin CE, Labelle H (2004) Patient-specific mechanical properties of a flexible multi-body model of the scoliotic spine. Med Biol Eng Comput 42:55–60

32. Larson AN, Polly DW, Diamond B et al (2014) Does higher anchor density result in increased curve correction and improved clinical outcomes in adolescent idiopathic scoliosis? Spine (Phila Pa 1976) 39:571–578

33. Kwan MK, Zeyada HE, Chan CY (2015) Prediction of curve correction using alternate level pedicle screw placement in patients with adolescent idiopathic scoliosis (AIS) Lenke 1 and 2 using supine side bending (SB) and fulcrum bending (FB) radiograph. Spine (Phila Pa 1976) 40:1605–1612

34. Keong KM, Aziz I, Yin Wei CC (2017) Prediction of height increment using preoperative radiological parameters following selective thoracic fusion with alternate-level pedicle screw construct in Lenke 1 and 2 adolescent idiopathic scoliosis patients. J Orthop Surg (Hong Kong) 25:2309499016684431

35. Cheung KM, Natarajan D, Samartzis D et al (2010) Predictability of the fulcrum bending radiograph in scoliosis correction with alternate-level pedicle screw fixation. J Bone Joint Surg Am 92:169–176

36. Le Naveaux F, Aubin CE, Larson AN et al (2015) Implant distribution in surgically instrumented Lenke 1 adolescent idiopathic scoliosis: does it affect curve correction? Spine (Phila Pa 1976) 40:462–468

37. Le Naveaux F, Aubin CE, Larson AN et al (2015) Key anchor points for specific correction maneuvers in Lenke 1 AIS: How important is the implant pattern design? In: SRS (ed) The 22nd international meeting on advanced spine techniques (IMAST), Kuala Lumpur, Malaysia

38. Havey RM, Voronov LI, Tsitsopoulos PP et al (2012) Relaxation response of lumbar segments undergoing disc-space distraction: implications to the stability of anterior lumbar interbody implants. Spine 37:733–740

39. Dang NR, Moreau MJ, Hill DL et al (2005) Intra-observer reproducibility and interobserver reliability of the radiographic parameters in the Spinal Deformity Study Group's AIS radiographic measurement manual. Spine 30:1064–1069

40. White KK, Oka R, Mahar AT et al (2006) Pullout strength of thoracic pedicle screw instrumentation: comparison of the transpedicular and extrapedicular techniques. Spine (Phila Pa 1976) 31:E355–E358

41. Pfeiffer M, Gilbertson LG, Goel VK et al (1996) Effect of specimen fixation method on pullout tests of pedicle screws. Spine (Phila Pa 1976) 21:1037–1044

42. Kwok AW, Finkelstein JA, Woodside T et al (1996) Insertional torque and pull-out strengths of conical and cylindrical pedicle screws in cadaveric bone. Spine (Phila Pa 1976) 21:2429–2434

43. Panjabi MM (1992) The stabilizing system of the spine. Part II: Neutral zone and instability hypothesis. J Spinal Disord 5:390–6 (discussion 7.).

44. Panjabi MM, White AA 3rd (1980) Basic biomechanics of the spine. Neurosurgery 7:76–93

45. Angelliaume A, Ferrero E, Mazda K et al (2017) Titanium vs cobalt chromium: what is the best rod material to enhance adolescent idiopathic scoliosis correction with sublaminar bands? Eur Spine J Off Publ Eur Spine Soc Eur Spinal Deform Soc Eur Sect Cerv Spine Res Soc 26:1732–1738

46. Huang TH, Ma HL, Wang ST et al (2014) Does the size of the rod affect the surgical results in adolescent idiopathic scoliosis? 5.5-mm versus 6.35-mm rod. Spine J Off J N Am Spine Soc 14:1545–1550

47. Cammarata M, Aubin CE, Wang X et al (2014) Biomechanical risk factors for proximal junctional kyphosis: a detailed numerical analysis of surgical instrumentation variables. Spine (Phila Pa 1976) 39:E500–E507

48. Aubin CE, Cammarata M, Wang X et al (2015) Instrumentation strategies to reduce the risks of proximal junctional kyphosis in adult scoliosis: a detailed biomechanical analysis. Spine Deform 3:211–218

49. Cheng I, Hay D, Iezza A et al (2010) Biomechanical analysis of derotation of the thoracic spine using pedicle screws. Spine 35:1039–1043

50. Parent S, Odell T, Oka R et al (2008) Does the direction of pedicle screw rotation affect the biomechanics of direct transverse plane vertebral derotation? Spine 33:1966–1969

51. Delikaris A, Wang X, Boyer L et al (2018) Implant density at the apex is more important than overall implant density for 3D correction in thoracic adolescent idiopathic scoliosis using rod derotation and en bloc vertebral derotation technique. Spine (Phila Pa 1976) 43:E639–E647

52. Le Naveaux F, Larson AN, Labelle H et al (2016) How does implant distribution affect 3D correction and bone-screw forces in thoracic adolescent idiopathic scoliosis spinal instrumentation? Clin Biomech (Bristol, Avon) 39:25–31